PRINTED TEM HORN ANTENNA FED BY BALANCED MICROSTRIP LINE

S. Lin[1, 2, *], X.-Q. Zhang[2], X.-Y. Zhang[2], and Y. Tian[2]

[1]Electronic Science and Technology Post-doctoral Research Center, Harbin Institute of Technology, Heilongjiang 150080, China

[2]School of Electronics and Information Engineering, Harbin Institute of Technology, Heilongjiang 150080, China

Abstract—In this paper, a new kind of printed TEM horn antenna with high-gain fed by balanced microstrip line is proposed. The radiation part of the antenna (printed on the FR4 epoxy substrate) is composed of two symmetrical triangular metal foil branches fed by balanced microstrip line. The antenna has been simulated by CST MICROWAVE STUDIO® software and the simulated results show that the proposed antenna is a kind of traveling wave antenna. Besides, an equivalent adopted V-shaped antenna model is proposed to describe the radiation characteristic of the antenna. The simulated and measured results indicate that in the frequency ranging from 1.64 GHz to 9 GHz, the reflection coefficient of the antenna is less than −6 dB and in the work frequency band, the average gain value is over 8.2 dB. The antenna gain will be improved greatly by extending the length of the dielectric slab appropriately (in the main radiation direction) without influencing the bandwidth. The measured and simulated results have a good consistency. This antenna will have wide application in the UWB field.

1. INTRODUCTION

Nowadays, ultra-wideband antenna research with the extension of the frequency spectrum of wireless instruments and a higher requirement for the bandwidth of antenna is raising more and more concerns. The ultra-wideband antenna has an extremely wide impedance bandwidth, thus several communication systems are able to share the same antenna which will reduce the number of antennas and volume

of the communication equipments. Moreover, the development of UWB technology promotes further researches on the time-domain characteristics of ultra-wideband antennas. Current ultra-wideband antennas mainly include log-periodic antenna [1], Archimedean spiral antenna [2], equiangular spiral antenna [3], bow-tie antenna [4], tear drop antenna [5], tapered slot antenna [6, 7], traditional TEM horn antenna [8–10], etc. Among them, traditional TEM horn antenna fails to benefit the integration of communication system because of its stereo-structure with relative big volume and heavy weight. The others could be designed as the structure of printed types to reduce the section and volume, and the antenna planarization can come into effect. The radiation models of Archimedean spiral antenna and equiangular spiral antenna are bidirectional circular polarization radiation. In order to attain one-way radiation of the antenna, the radiator reflector must be increased at the cost of heightening antenna section. Bow-tie antenna and tear drop antenna have omnidirectional liner polarization radiation structures. In order to realize their directional radiation, these antennas need to compose relevant antenna array or add reflectors at the cost of introducing a complex feeding network. The log-periodic antenna is usually fed from the short dipole side, and the directional radiation can be realized by overlapping feeding. However, it will introduce a length of coaxial line so that the application in the millimeter-wave and integrated circuits will be restricted. In addition, tapered slot antenna is a planar printed type of antenna, and it usually consists of feeding network and radiator. Furthermore, the plane figure of the radiator is similar to the projection on the E plane of TEM horn antenna with adding ridge. Consequently, the tapered slot antenna can be classified as planar TEM horn antenna. These antennas can be divided into Vivaldi antenna, LTSA antenna [11–13] and others, according to different tapered forms of the slot lines. All of them have relatively complex structures with ultra-wideband and balanced feeding.

Different researchers have different opinions about the definition of UWB antennas. It is usually considered that an antenna with a ratio bandwidth (ratio of the upper and lower limit working frequencies) over 2 : 1 can be called as a UWB antenna. The frequency range of the civil UWB communication with band of 3.1–10.6 GHz (ration bandwidth is 3.42 : 1) proposed by FCC has gained wide attention. Researchers have designed a lot of antenna working in this band, and antennas in this type all have ratio bandwidth over 3.42 : 1.

In this paper, a new kind of printed TEM horn antenna with high-gain fed by balanced microstrip line is proposed. The radiation part of the antenna consists of two symmetrical triangular metal foil

branches which are printed on the FR4 epoxy resin substrate and fed by balanced microstrip line. The antenna has been simulated by CST MICROWAVE STUDIO® software, and the parameters are gained. The simulated and experimental results indicate that in the operating frequency band from 1.64 GHz to 9 GHz, the ratio bandwidth is 5.5 : 1. Additionally, the antenna has stable directional radiation characteristics, and the feeding structure is simple. The analysis of the simulation and experiment results are shown in the paper.

2. THE DESIGN OF THE ANTENNA

The whole antenna (shown in Fig. 1) consists of a feeding part and a radiation part, while the radiation part is composed of metal radiator and medium focusing part. The medium focusing part has a novel structure introduced into planar TEM horn antenna in this paper. With such a structure, the electronic field energy density will be enhanced, so that the antenna gain can be greatly increased. The metal radiator can be regarded as a gradually opening slot line. The design of the metal radiator can be calculated according to the relative formula in [14], and the obtained value can be set as the initial value of the simulation.

The feeding part is a balanced microstrip line, and the original port impedance of the feed port is $50\,\Omega$. Moreover, the joint port

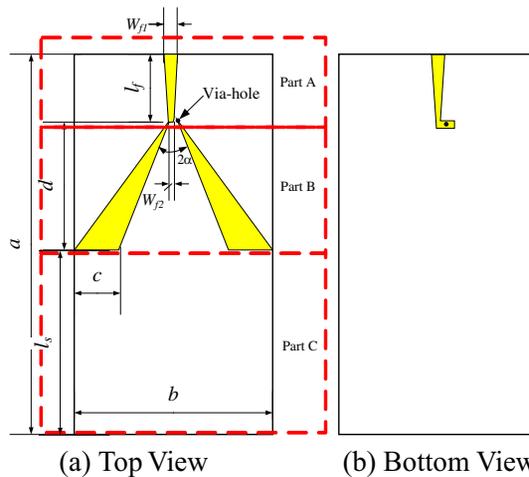(a) Top View   (b) Bottom View

Figure 1. Sketch of the proposed antenna (Part A: feeding part, Part B: metal radiator, Part C: medium focusing part).

Table 1. Antenna parameters.

Parameters	Value
Dielectric slab length a	213 mm
Dielectric slab width b	120 mm
Dielectric slab height h	1.5 mm
Dielectric slab reflection coefficient ε_r	4.4
Dielectric slab Loss Tangent	0.025
Triangular radiator bottom line length c	30 mm
Triangular radiator height d	73 mm
Feeding length l_f	35 mm
Feeding port feeding length w_{f1}	2 mm
Radiator port feeding length w_{f2}	0.8 mm
Focusing part length l_s	100 mm

impedance between the terminal of the feeding line and the antenna should match the imputing port. And the input impedance of antenna radiator equals the input impedance of the tapered slot line which is open-ended (200 Ω). Thus the balanced microstrip line should also be designed as a tapered form. The major parameters depend on the ratio of the width and height and reflection coefficient of the dielectric substrate slab. Their characteristic impedance calculation method can be referred by the method of calculating characteristic impedance of the microstrip line. Thereforethe fundamental parameters of the antenna are shown in Table 1.

3. SIMULATION ANALYSIS

3.1. Ultra-wideband Characteristics

Most antennas consist of feeding line and radiator. An antenna can achieve ultra-wideband characteristics only when the radiator has the ultra-wideband impedance characteristics. The balanced microstrip line in this paper is a kind of TEM wave transmission line which has ultra-wideband transmission characteristics. Therefore, the ultra-wideband characteristics of the antenna can be analyzed through surface current distribution of the transmission line. The
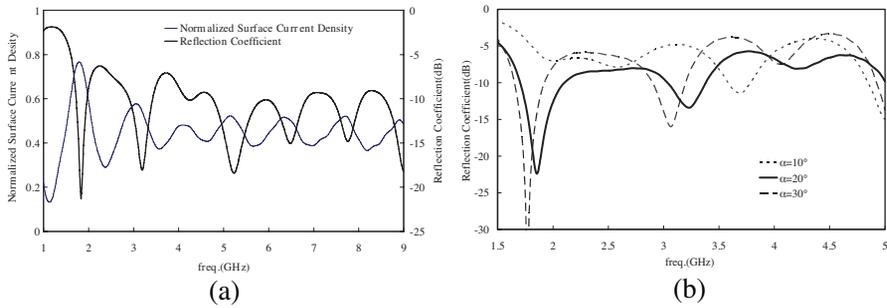
Figure 2. Surface current density and reflection coefficient of the antenna. (a) Surface current density and reflection coefficient at the feeding point. (b) Influence of angle α on antenna's reflection coefficient.

antenna model which is set up according to the structure in Fig. 1 and parameters in Table 1 has been simulated by CST software. The simulated results of the surface current density on the antenna radiation feeding line and the feeding terminal connecting with antenna radiator (shown in Fig. 2(a)) indicate that the surface current density is a wideband traveling current so that the ultra-wideband characteristics of the antenna are reflected. Besides, the simulated results of reflection coefficient shown in Fig. 2(a) indicate ultra-wideband characteristics of the antenna (in the work frequency band from 1.64 GHz to 9 GHz reflection coefficient is less than -6 dB the standing wave coefficient is less than 3.0) because the feeding line of the antenna is TEM wave transmission line, and antenna radiator of the antenna can be regarded as the slot line gradually opening, which is also an ultra-wideband transmission line. The whole antenna can be viewed as the structure of "Tapered balance microstrip line-Tapered slot line-Free space". Such three components of this structure are all ultra-wideband, so the antenna is with the ultra-wideband characteristics.

The value of angle 2α between two branches of the slot line changing gradually has great effect on the reflection coefficient. And the final angle is determined by the simulated results. Antenna reflection coefficients with different *lapha* values are shown in Fig. 2(b). The figure indicates that there exists a best value of α to make antenna reflection coefficient the lowest. In the design of antenna in this paper, the index of reflection coefficient is firstly satisfied, and it is also the most important one. Thus, through further simulation, the final angle is $\alpha = 22°$.
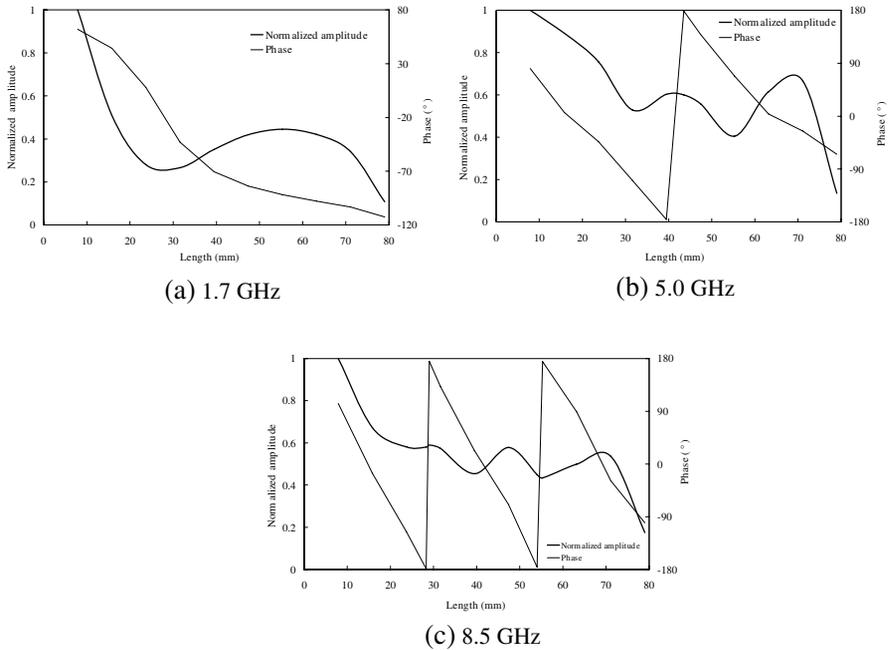
Figure 3. Distribution of the antenna surface current.

3.2. Directional Radiation Characteristics

For the metal radiator, metal surface current is the main cause of the radiation. In Fig. 3, main surface currents that may generate radiation (named $i_1 - i_4$) are listed. Among them, currents i_1 and i_4 distribute on the upper and lower branches of the transmission line, and generally they hardly generate radiation. The radiation is mainly caused by i_2 and i_3. The flowing physical length of current i_2 and i_3 have the same length of 78.9 mm calculated by the dimension of the mental radiator. Amplitude and phase distributions of the surface current density in the length at frequency points of 1.7 GHz, 5.0 GHz and 8.5 GHz are simulated separately (shown in Fig. 3). For the above three frequencies, the electrical sizes of the antenna radiator's physical length are 0.45λ, 1.32λ and 2.24λ.

It is found in the simulation that, considering the flowing current direction, the amplitude and phase distributions of the two main radiating currents i_2 and i_3 are the same. However, the directions differ by 180°. Therefore, Fig. 4 just shows the amplitude and phase distribution of i_2. The amplitude distribution of the current shows that there is no wave node in length over one wavelength (at 5.0 GHz and 8.5 GHz), and it indicates that the current distributions on the antenna radiator at such three frequencies are all traveling wave distribution. Besides, the current phase distribution also proves the same point. The current phase shifts at these three frequencies on the radiator are 174.5°, 505.9°, and 923.9°.

In the calculations of the currents in radiator edge and phases in different frequencies, we should note that the phases shown in Figs. 4(a)–(c) are the main values of the arguments of complex i_2, and the changing range of main values of the arguments is from −180° to

(a) 1.7 GHz

(b) 5.0 GHz

(c) 8.5 GHz

Figure 4. Amplitude and phase distributions of i_2 at three selected frequencies.

$+180°$. Therefore, additional integer times of $360°$ are needed in the phase calculations. For example, the phase is changing consistently with no jump in Fig. 4(a). Thus the phase value can be gained as $174.5°$ only by terminal phase subtracting initial phase. And Fig. 4(b) shows that the phase value has one jump and gradually decreases to $-180°$, and the changing phase value is $260.95°$. Then the value jumps to $+180°$ and gradually decreases to get a phase change of $244.9°$. Therefore, the total phase change is $260.95° + 244.9° = 505.9°$ when current i_2 working at $5.0\,\text{GHz}$. Similarly, the picture shown in Fig. 4(c) indicates that the phase value has jumped twice and that additional phase of $360°$ is needed in calculation. Thus the final calculation result is $923.9°$.

Accordingly, this TEM horn antenna can be equivalent to a typical traveling wave antenna — V-shaped antenna. So the antenna radiation can be explained by the synthetic model of the two sections of traveling-wave single-wires which compose the V-shaped antenna (shown in Fig. 3).

Shown in Fig. 3, the radiation of the antenna is provided by two

radiating arms supporting currents i_2 and i_3. Previous simulation results indicate that the amplitudes and phases distribution of i_2 and i_3 along the linear direction are basically the same. Thus, the same expression can be used to describe:

$$I(l_2) = I_0 e^{-j\zeta k l_2} \tag{1}$$

In the expression, I_0 is the current at $y = 0$, and $\zeta = \frac{c}{v}$ is the slow-wave coefficient. $I(l_2)$ is the current value after the length of l_2. And l_2 is the path that i_2 flows (l_2 the distance between Δi_2 and O point in Fig. 3).

$$y = l_2 \cos \alpha \tag{2}$$

$$I\left(\frac{y}{\cos \alpha}\right) = I_0 e^{-j\zeta k \frac{y}{\cos \alpha}} \tag{3}$$

According to expression (3), radiation field, generated by currents i_2 and i_3, can be calculated separately. Then by adding them up, the radiation field of the proposed antenna in this paper can be obtained. Note that when calculating the total field generated by stacking, the effect on the total field generated by the phase changes (caused by the position) should be taken into full consideration. Because the directions of the two traveling wave currents are different, instead of the principle of pattern multiplication, only the method of vector superposition could be used.

Detailed solution is shown as follows:

1. Radiation field of the micro-unit

In Fig. 3, the radiation field generated by the current micro-unit Δi_2 (length Δl_2) is:

$$\Delta E_{\delta_2} = j\frac{60\pi \Delta i_2(\Delta l_2)}{\lambda r_{\Delta i_2}} \sin \delta_2 e^{-jk r_{\Delta i_2}} \tag{4}$$

The radiation field generated by the current micro-unit Δi_3 (length Δl_3) is

$$\Delta E_{\delta_3} = j\frac{60\pi \Delta i_3(\Delta l_3)}{\lambda r_{\Delta i_3}} \sin \delta_3 e^{-jk r_{\Delta i_3}} \tag{5}$$

The relationship between the locations of the two current micro-units Δi_2 and Δi_3 can be expressed by the following formula (6)–(14):

$$y_{\Delta i_2} = y_{\Delta i_3} \tag{6}$$

$$r_{\Delta i_2} = r_0 - \frac{y}{\cos \alpha} \cos \delta_2 = r_0 - \frac{y}{\cos \alpha} \cos(\varphi - \alpha) \tag{7}$$

$$r_{\Delta i_3} = r_{\Delta i_2} + (2y \tan \alpha) \sin \varphi = r_0 - \frac{y}{\cos \alpha} \cos \delta_2 + 2y \tan \alpha \sin \varphi$$

$$= r_0 - \frac{y}{\cos \alpha} \cos(\varphi - \alpha) + 2y \tan \alpha \sin \varphi \tag{8}$$

$$\delta_2 = \varphi - \alpha \tag{9}$$

$$\delta_3 = \varphi + \alpha \tag{10}$$

$$\Delta l_2 = dy/\cos\alpha \tag{11}$$

$$\Delta l_3 = dy/\cos\alpha \tag{12}$$

$$(\Delta E_{\delta_i})_x = -\Delta E_{\delta_i}\cos\varphi, \quad i = 2,3 \tag{13}$$

$$(\Delta E_{\delta_i})_y = -\Delta E_{\delta_i}\sin\varphi, \quad i = 2,3 \tag{14}$$

The explanations of the above variables are as follows (refer to Fig. 3):

$r_{\Delta i_2}$ — distance between the current micro-unit Δi_2 and far-field observation point;

$r_{\Delta i_3}$ — distance between the current micro-unit Δi_3 and far-field observation point;

r_0 — distance between O point and far-field observation point;

2α — angle between traveling current i_2 and i_3;

φ — angle between r_0 and y axis;

δ_2 — angle between $r_{\Delta i_2}$ and i_2;

δ_3 — angle between $r_{\Delta i_3}$ and i_3;

2. The total radiation field x direction component $(E_{\text{total}})_x$ and y direction component $(E_{\text{total}})_y$ on the xy plane (antenna E-plane)

$$(E_{\text{total}})_x = \int_0^d [(\Delta E_{\delta_2})_x + (\Delta E_{\delta_3})_x] \tag{15}$$

$$(E_{\text{total}})_y = \int_0^d [(\Delta E_{\delta_2})_y + (\Delta E_{\delta_3})_y] \tag{16}$$

Finally, the power directivity function on the xy plane of the antenna is:

$$P(\varphi) = \text{Re}_x^2 + \text{Im}_x^2 + \text{Re}_y^2 + \text{Im}_y^2 \tag{17}$$

In the expression,

$$\text{Re}_x = A_1\cos(kdB) - A_2\cos(kdC) - (A_1 - A_2) \tag{18}$$

$$\text{Im}_x = -A_1\sin(kdB) + A_2\sin(kdC) \tag{19}$$

$$\text{Re}_y = A_3\cos(kdB) - A_4\cos(kdC) - (A_3 - A_4) \tag{20}$$

$$\text{Im}_y = -A_3\sin(kdB) + A_4\sin(kdC) \tag{21}$$

$$A_1 = \frac{\cos\varphi\sin(\varphi - \alpha)}{B} \tag{22}$$

$$A_2 = \frac{\cos\varphi\sin(\varphi + \alpha)}{C} \tag{23}$$

$$A_3 = \frac{\sin\varphi \sin(\varphi - \alpha)}{B} \tag{24}$$

$$A_4 = \frac{\sin\varphi \sin(\varphi + \alpha)}{C} \tag{25}$$

$$B = \frac{\zeta - \cos(\varphi - \alpha)}{\cos\alpha} \tag{26}$$

$$C = B + 2\tan\alpha \sin\varphi \tag{27}$$

3. The total radiation field (with only x direction component) on the yz plane (H-plane of the antenna)

$$(E_{\delta_i})_x = E_{\delta_i}(\delta_i = \alpha), \quad i = 2, 3 \tag{28}$$

The relationship between the locations of the two micro-units can be expressed by the following formulas (29)–(30):

$$\cos\varphi = \frac{\cos\delta_i}{\cos\alpha}, \quad i = 2, 3 \tag{29}$$

$$r_0 - r_i = y\frac{\cos\delta_i}{\cos\alpha}, \quad i = 2, 3 \tag{30}$$

φ is the angle between the directions of viewing direction (r_0) and maximum radiation ($+y$).

Finally, the power directivity function on the yz plane of the antenna is:

$$P(\varphi) = \left(\frac{\sin\frac{kdB_H}{2}}{\frac{kdB_H}{2}}\right)^2 \tag{31}$$

In the expression, $B_H = \zeta/\cos\alpha - \cos\varphi$.

Based on the above expressions, the power pattern (or the field strength pattern) of the antenna in xy plane and yz plane can be calculated. Then both of the calculated pattern and simulated one are drawn in Fig. 5. The conclusions can be drawn as followed: (1) Both of the calculated and simulated results indicate that the antenna is directional. The validity of proposed equivalent V-shaped antenna is proved. (2) The main lobe of calculated results in the pattern is larger than that of the simulated ones. Especially, the main lobes of H plane at 1.7 GHz and 5.0 GHz have larger errors because the radiation generated by the current (in X axis) on the bottom margin of the triangular branches is considered in calculation. This current will also influence the calculated results although its amplitude is small. (3) The calculated and simulated results of the side and back lobe in the pattern differ a lot because the influences of the medium and radiation generated by the current at the triangular patches' lateral edge are not taken into consideration. (4) Although the calculated and simulated
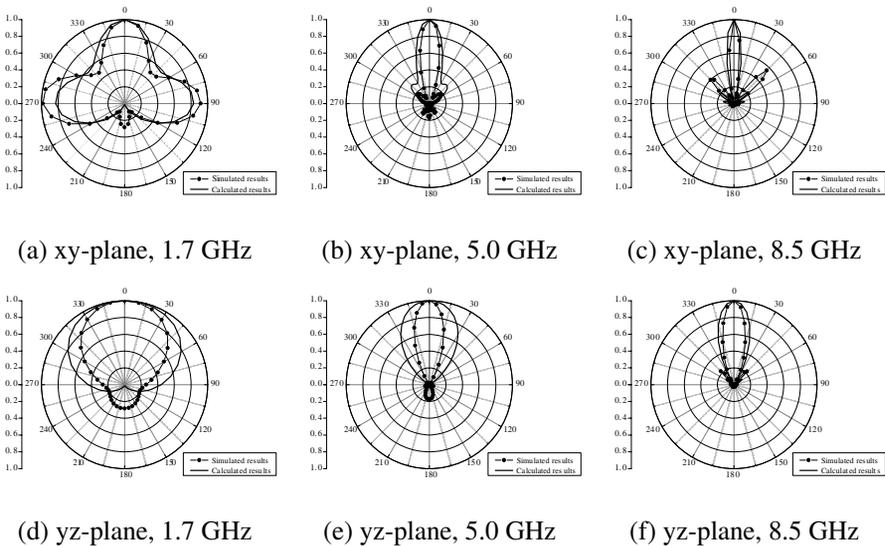
(a) xy-plane, 1.7 GHz (b) xy-plane, 5.0 GHz (c) xy-plane, 8.5 GHz

(d) yz-plane, 1.7 GHz (e) yz-plane, 5.0 GHz (f) yz-plane, 8.5 GHz

Figure 5. Comparison between the simulated and calculated results of antenna pattern.

results have differences, their trends are very anastomosing. Thus, the mode of the equivalent V-shaped antenna can well simulate and explain the characteristics of the antenna in this paper. This mode can also explain similar antennas, for example, Vivaldi antenna, LTSA, etc.

According to the simulated and calculated results, the main reason that the antenna can have characteristic of directional radiation is that the radiation of traveling wave current could form two main lobes on the E-plane. The two main lobes will lean to the side lagging of the current phase. Therefore, the main lobe fields of the two traveling wave currents will be added up to form a new main lobe by making the two traveling waves form a V-shape as well as selecting the included angle properly. Then the directional radiation of the antenna can be achieved.

In addition, the side lobe of the E-plane pattern at higher frequencies is greater and relatively close to the main lobe because there are two E-plane main lobes formed by the radiation of traveling wave current, so the higher the frequency is, the smaller the included angle between the maximum radiation-directions of the two main lobes will become. However, after the two traveling wave currents form the V-shaped antenna, each main lobe will form a new one in the far field zone, and other main lobes will form side lobes. Thus, an effect similar to the pattern splitting at high frequencies will be generated. As a

result, the application of this antenna will be limited, and the radiation pattern bandwidth would be less than its impedance bandwidth.

3.3. High-gain Characteristics

Simulation, focusing on influence on antenna gain, is done on the length of the dielectric slab in radiation direction. The simulated results are presented, and $l_s = 0$, 50 mm, 100 mm and 150 mm is taken in Fig. 6. The results indicate that after lengthening the dielectric slab, antenna gain is obviously improved. And the length of the dielectric slab and antenna gain are of positive correlation. For the proposed antenna in this paper, the value of the length of the dielectric slab is 100 mm (compared to $l_s = 0$, the gain increases by 3.9 dB, which has the largest difference in-band). Furthermore, in the simulation process, there is almost no influence on the antenna wideband with such a method to improve the gain.
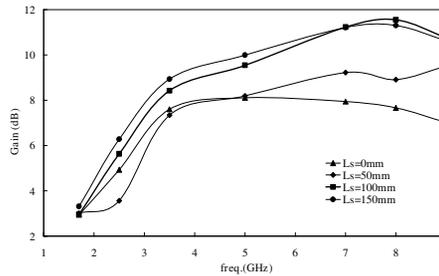
Figure 6. The effects of antenna gain with varying length l_s of the extended dielectric slab.

(a) Front   (b) Back

Figure 7. Prototype of the proposed antenna.

4. EXPERIMENTAL RESULTS

According to the acquired antenna parameters, prototype of the proposed antenna (shown in Fig. 7) has been manufactured and measured in the anechoic chamber with the Agilent E8363B vector network analyzer. Reflection coefficient, radiation pattern and gain are included in the measuring content, and the measured results are shown in Figs. 8 to 10. The experimental results show that the reflection coefficient of the proposed antenna is less than -6 dB (standing wave coefficient less than 3.0) in the frequency band of 1.6–9 GHz, and the reflection coefficient is less than -8 dB (standing wave coefficient less than 2.3) in 2.7–6.8 GHz. This measured results basically accord with the simulated ones. The value of the measured gain is smaller by 1–2 dB than the simulated one. The measured and simulated results of the radiation pattern have slight difference in the main-lobe area, while have a relatively large difference in the side-lobe. In general, the antenna property meets the characteristics of ultra-wideband antenna. And the reasons for the difference between the simulated and measured results can be explained as the following: (1) The printed substrate is normal FR4 epoxy resin substrate which has large loss, and the loss tangent is about 10^{-2} order of magnitude, much larger than the
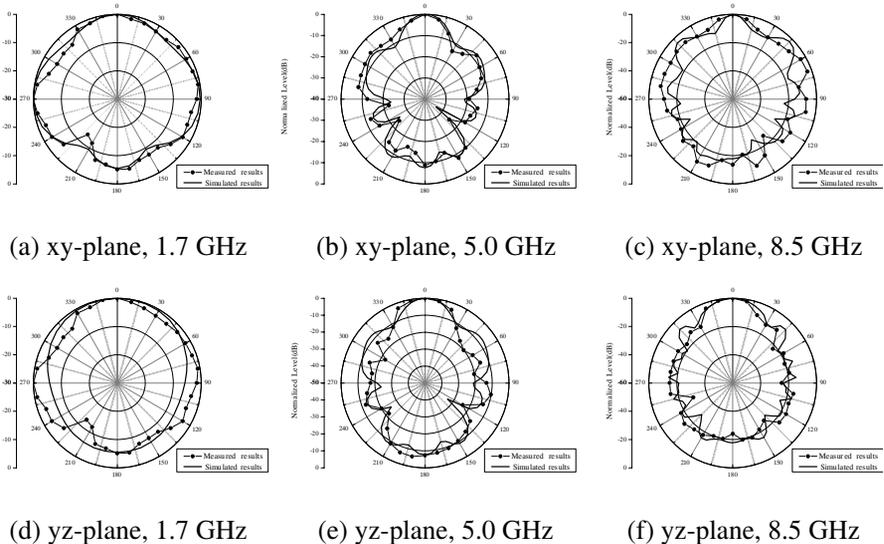

   (a) xy-plane, 1.7 GHz   (b) xy-plane, 5.0 GHz   (c) xy-plane, 8.5 GHz

   (d) yz-plane, 1.7 GHz   (e) yz-plane, 5.0 GHz   (f) yz-plane, 8.5 GHz

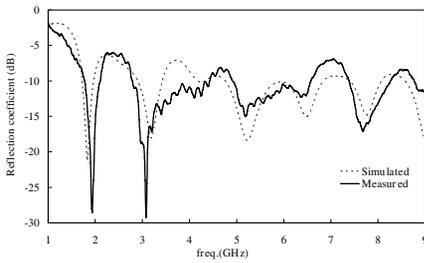**Figure 8.** Comparison between the simulated and measured results of antenna pattern.

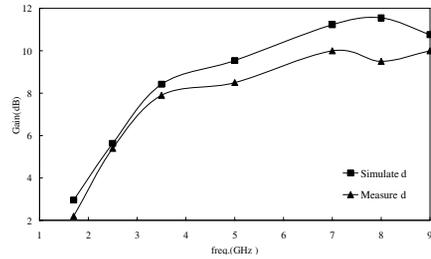**Figure 9.** The measured results of reflection coefficient.

Figure 10. Antenna gain curve.

common Rogers series materials (10^{-4} order of magnitude). So the resulted energy loss will lead to the decrease of reflection coefficient and gain. (2) Antenna weld and radiation-pattern test fixture will influence the measured results of the side-lobe voltage level. Besides, the measured results of the antenna radiation pattern will be also influenced by the instability of FR4 substrate.

Note that the reason for the difference between the traditional V type traveling antennas and the antenna in this paper is that the antenna is printed on the FR4 epoxy resin lamina with dielectric loss (loss tangent $\tan \delta = 0.025$) and that the radiation caused by currents on the radiator part will be absorbed by surrounding dielectric. Thus, the antenna reflection coefficient is decreased, and the ultra wide band effect can form. Compared to the matched load with loading lumped parameters of traditional V type antenna, the antenna in this paper is equal to the matched load with loading distributed parameters. The results of doing so will make the proposed antenna similar to axial mode spiral antenna and utilize the radiation of antenna's radiator to achieve matching. But it will lead to the decrease of antenna efficiency.

5. CONCLUSION

In this paper, a printed high-gain TEM horn antenna high-gain fed by balanced microstrip line is proposed. The proposed antenna is a traveling-wave antenna and does not introduce lossy matched load. The surface current of the metal antenna has been simulated and analyzed, and the ultra-wideband characteristics of the antenna are explained. Moreover, according to the simulation results of the metal radiator surface current, the V-shaped traveling-wave antenna model with equal radiation characteristics to the TEM horn antenna is proposed, and the directivity-function analytical expression of the antenna is deduced to explain the directional radiation characteristics.

The results also indicate that extending the length in the radiation direction of the dielectric slab could enhance the antenna gain without influencing the antenna bandwidth and that this method is a superior way to obtain high antenna gain. The experimental results show that the antenna can operate at 1.64 GHz to 9 GHz with the average gain of 8.2 dB, so this antenna can be widely applied in the UWB field. Moreover, the balanced microstrip line method can avoid the introduction of a coaxial line. Consequently, this proposed antenna can be applied to the millimeter-wave and integrated circuit system field.

ACKNOWLEDGMENT

REFERENCES

1. Baek, Y.-H., L. H. Truong, S.-W. Park, S.-J. Lee, Y.-S. Chae, E.-H. Rhee, H.-C. Park, and J.-K. Rhee, "94-GHz log-periodic antenna on GaAs substrate using air-bridge structure," *IEEE Antennas and Wireless Propagation Letters*, Vol. 8, 909–911, 2009.

2. Chen, T.-K. and G. H. Huff, "Stripline-fed archimedean spiral antenna," *IEEE Antennas and Wireless Propagation Letters*, Vol. 10, 346–349, 2011.

3. Nakano, H., K. Kikkawa, N. Kondo, Y. Iitsuka, and J. Yamauchi, "Low-profile equiangular spiral antenna backed by an EBG reflector," *IEEE Transactions on Antennas and Propagation*, Vol. 57, No. 5, 1309–1318, May 2009.

4. Lestari, A. A., E. Bharata, A. B. Suksmono, A. Kurniawan, A. G. Yarovoy, and L. P. Ligthart, "A modified bow-tie antenna for improved pulse radiation," *IEEE Transactions on Antennas and Propagation*, Vol. 58, No. 7, 2184–2192, Jul. 2010.

5. Abe, H., H. Tanaka, M. Tokuda, and S. Ishigami, "Optical feeding antenna with wide bandwidth for evaluation of radiated emission test sites above 1 GHz," *Electromagnetic Compatibility, IEEE International Symposium on Digital Object Identifier*, 1–6, 2008.

6. Pazin, L. and Y. Leviatan, "A compact 60-GHz tapered slot antenna printed on LCP substrate for WPAN application," *IEEE Antennas and Wireless Propagation Letters*, Vol. 9, 272–275, 2010.

7. Cheng, Y. J., W. Hong, and K. Wu, "Design of a monopulse antenna using a dual V-type linearly tapered slot antenna (DVLTSA)," *IEEE Transactions on Antennas and Propagation*, Vol. 56, No. 9, 2903–2909, Sep. 2008.

8. Ranga, Y., A. K. Verma, and K. P. Esselle, "Planar-monopole-fed, surface-mounted quasi-TEM horn antenna for UWB systems," *IEEE Transactions on Antennas and Propagation*, Vol. 58, No. 7. 2436–2439, Jul. 2010.

9. Peytavit, E., J.-F. Lampin, T. Akalin, and L. Desplanque. "Integrated terahertz TEM horn antenna," *Electronics Letters*, Vol. 43, No. 2, 73–75, 2007.

10. Wu, F.-T. and N.-C. Yuan, "The radiation characteristic of UWB planar TEM horn antenna array," *International Conference on Radar*, 1–4, 2006.

11. Che, Y., K. Li, X. Hou, and W. Tian, "Simulation of a small sized antipodal vivaldi antenna for UWB applications," *IEEE International Conference*, Vol. 1, 1–3, 2010.

12. Lin, S., S. Yang, and A. E. Fathy, "Development of a novel UWB vivaldi antenna array using SIW technology," *Progress In Electromagnetics Research*, Vol. 90, 369–384, 2009.

13. Radenamad, D., T. Aoyagi, and A. Hirose, "Low impedance bulk LTSA," *IEEE Electronics Letters*, Vol. 46, 882–883, 2010.

14. Janaswmy, R. and D. H. Schaubert, "Characteristic impedance of a wide slot line on low-permittivity substrates," *IEEE Transactions on Antennas and Propagation*, Vol. 34, 900–902, 1986.